ELSEVIER

International Journal of Mass Spectrometry 213 (2002) 91–99

www.elsevier.com/locate/ijms

**Accelerated communication**

# Atmospheric peroxy radicals: ROXMAS, a new mass-spectrometric methodology for speciated measurements of $HO_2$ and $\Sigma RO_2$ and first results

M. Hanke[a], J. Uecker[a], T. Reiner[a], F. Arnold[a]

[a]*Max-Planck Institute for Nuclear Physics, Atmospheric Physics Division, Heidelberg, Germany*

Received 3 September 2001; accepted 15 October 2001

**Abstract**

ROXMAS (ROx Chemical Conversion/CIMS), a novel method for atmospheric speciated measurements of $HO_2$ and the sum of organic peroxy radicals ($\Sigma RO_2$) developed by MPI-K, has been successfully deployed in a field campaign on Monte Cimone, Italy, June–July 2000. The method relies on amplifying chemical conversion of peroxy radicals to gaseous sulfuric acid via the chain reaction with NO and $SO_2$ and detection of the sulfuric acid by CIMS. Speciated measurements have been realized by diluting atmospheric air in either $N_2$ or $O_2$ buffer, thus exploiting the dependence of the conversion efficiency of $RO_2$ to $HO_2$ on [$O_2$], [NO], and [$SO_2$]. Speciated measurements of $HO_2$ and $RO_2$ are required to provide further insight into radical partitioning and thus to elucidate further the mechanisms of the oxidation of volatile organic compounds in the troposphere. This methodology yields useful speciated results for atmospheric conditions where $CH_3O_2$ makes a major contribution to total $RO_2$. Under other conditions it gives an upper limit for [$HO_2$] and a lower limit for [$\Sigma RO_2$]. (Int J Mass Spectrom 213 (2002) 91–99) © 2002 Elsevier Science B.V.

*Keywords:* ROXMAS, chemical flow reactor; Chemical ionization mass spectrometry (CIMS); $HO_2$ radical; $RO_2$ radical; Atmospheric speciated measurements

## 1. Introduction

Catalytic reaction cycles involving free radicals are the driving force in the tropospheric oxidation of many gaseous species to compounds that are more easily scavenged and removed by aerosols, clouds, and rain. During the day most of the reaction cycles are initiated by reactions of the hydroxyl radical (OH) resulting from UV photodissociation of $O_3$ at wavelengths shorter than 318 nm. Hydroperoxy radicals ($HO_2$) and organic peroxy radicals ($RO_2$ with R being an organic group, e.g. $CH_3$) are the key reactive intermediates/chain propagators. Oxidation of CO and hydrocarbons by OH leads to the formation of $HO_2$ and $RO_2$, respectively. Reactions of $HO_2$ with NO or $O_3$ recycle OH from $HO_2$. $RO_2$ is converted to $HO_2$ by reacting with NO. These cycling reactions establish a rapid steady state for OH, $HO_2$, and $RO_2$

* Corresponding author. E-mail:markus.hanke@mpi-hd.mpg.de


*PII* S1387-3806(01)00548-6

(lifetime of OH ~ 1 sec, lifetime of peroxy radicals ~1 min) [1,2] At nighttime formation and evolution of the radical pool may occur by ozonolysis of volatile organic compounds (VOCs) or reactions of VOCs with $NO_3$ [3].

The knowledge of the abundance and distribution of $RO_x$ ($RO_x$ = OH + $HO_2$ + $RO_2$) species is necessary for a better understanding of tropospheric oxidation chemistry, such as the atmospheric degradation of VOCs, the production and destruction of ozone or the nighttime oxidation processes. The ratio $RO_2/HO_2$ reflects the interconversion reactions and thus is a useful parameter in tests of atmospheric chemistry models.

Only in the recent past reliable methods for the ambient monitoring of the highly reactive and thus short-lived peroxy radicals have emerged: Laser-induced fluorescence (LIF) [4–10], Chemical Amplification [11–13], and matrix isolation/electron spin resonance (MIESR) [14].

For aircraft-borne and ground-based measurements of atmospheric peroxy-radical concentrations a novel method has been introduced by our group [15–19]. This method, ROxMAS ($RO_x$ chemical conversion/chemical ionization mass spectrometry), relies on amplifying chemical conversion of peroxy radicals to gaseous sulfuric acid that is detected by CIMS. Recently we have developed a new mode of operation allowing on-line speciated measurements of $HO_2$ and $HO_2$+$RO_2$ [19–22] with a time resolution of 1 min and a sensitivity of 0.5 pptv. ROxMAS was automated to allow continuous long-term measurements.

In the present paper we describe instrumental aspects of the ground-based computer-controlled ROxMAS system and report on recent speciated field measurements of $HO_2$ and $RO_2$.

## 2. ROxMAS

### 2.1. Measurement principle

The basic reactions involved in amplifying chemical conversion of peroxy radicals to $H_2SO_4$ via reactions with NO and $SO_2$ in a flow reactor are summarized in Fig. 1. The recycling of $HO_2$ in the reaction of $HSO_3$ with $O_2$ initiates a chain reaction leading to an amplified $H_2SO_4$ signal exceeding the peroxy-radical concentration. The chain reaction is terminated by the reaction of OH with NO. The final $H_2SO_4$ concentration [$H_2SO_4$] is determined by the relative rates of the competing reactions of OH with $SO_2$ (chain carrying reaction) and with NO (chain terminating reaction). The ratio of the two reaction rates gives the chain length (CL) and is equal to the ratio between the final [$H_2SO_4$] and the peroxy-radical concentration.

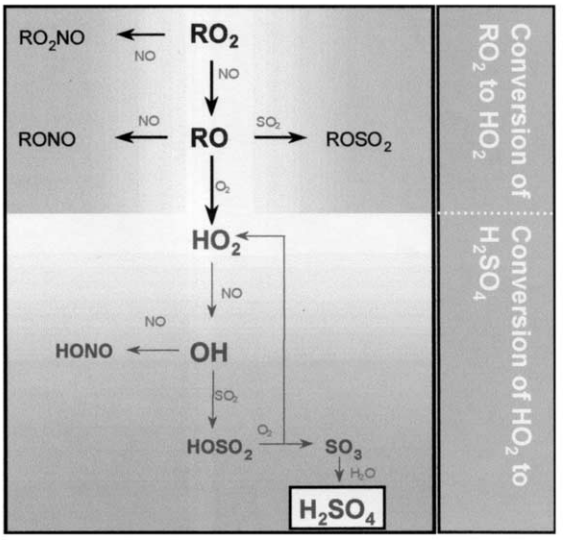


Fig. 1. Simplified illustration of the conversion mechanism of simple organic peroxy radicals $RO_2$ to $HO_2$ under conditions present in the ROxMAS flow reactor. Possible isomerization and decomposition processes of the more complex organic radicals are neglected and not shown.

$$[H_2SO_4] = [HO_2 + RO_2] \times \frac{k_{OH+SO2} \times [SO_2]}{K_{OH+NO} \times [NO]} = [HO_2 + RO_2] \times CL \quad (1)$$

For the commonly used operational conditions, the high sensitivity of CIMS and the low atmospheric background of gaseous $H_2SO_4$ allow for work with short chain lengths of the order of 10 to 15 and short reaction times of 0.1s for the entire conversion and amplification process. This reduces the impact of potential interference and loss processes due to either

reactions of other ambient trace gases such as chain terminating reactions other than the reaction of OH with NO (e.g. reaction of OH or $HO_2$ with ambient $NO_2$ or $NO_2$ resulting from the reaction of ambient $O_3$ with NO added as reagent gas into the flow reactor) or wall losses of the radicals on the surfaces of the flow-reactor walls [17,19,21].

Organic peroxy radicals ($RO_2$) are converted to $HO_2$ by reactions with NO and $O_2$. In a high NO and $SO_2$ environment ([NO]≈$10^{13}$ $cm^{-3}$ and [$SO_2$]≈ $10^{15}$ $cm^{-3}$) as used in our flow reactor, addition reactions of $RO_2$ with NO and of RO with NO and $SO_2$, however, may compete with the conversion path (Fig.1). The conversion efficiency (CE) of $RO_2$ to $HO_2$ depends on the concentrations of $O_2$, NO, $SO_2$, the relative reaction rates, and the organic group R. For simple peroxy radicals [21,23,24] (e.g. R=$CH_3$ or $C_2H_5$), whose subsequently formed oxy-radicals RO do not undergo isomerization or decomposition, the conversion efficiency can be reduced to

$$\mathrm{CE} \approx \frac{k_{RO_2+NO}}{k_{RO_2+NO} + k_{RO_2+NO+M}} \times \frac{k_{RO+O_2} \times [O_2]}{k_{RO+O_2} \times [O_2] + k_{RO+SO_2+M} \times [SO_2] + k_{RO+NO+M} \times [NO]} \quad (2)$$

Eq. (2), which is radical dependent [23,24], can be exploited to discriminate between $RO_2$ and $HO_2$ by either decreasing or increasing CE by dilution of the sampled air with a buffer gas, either $N_2$ or $O_2$, respectively. In the case of $N_2$ as buffer, the $O_2$ concentration in the flow reactor is reduced to such an extent (∼2%) that the conversion of RO to $HO_2$ is suppressed and the addition reactions become dominant. In this case the $H_2SO_4$ mainly stems from conversion of ambient $HO_2$ ("$HO_2$-only mode"). In the case of $O_2$ as buffer, the $O_2$ concentration is elevated (>70%) and the conversion of RO to $HO_2$ is favored against the addition reactions; thus both $HO_2$ and $RO_2$ are measured ("$HO_2$+$RO_2$ mode"). For the two cases, [$H_2SO_4$] can be expressed as

$$[H_2SO_4]_{buffer} = \alpha_{HO_2} \times [HO_2] + \sum_i \alpha_{R_iO_2} \times \mathrm{CE}_{i(buffer)} \times [R_iO_2] \quad (3)$$

The alpha factors, with values on the order of 0.1, comprise the chain length [see Eq. (1)] of the conversion and amplification mechanism, the pressure, dilution and temperature correction with respect to the difference between ambient conditions and flow-reactor conditions. Furthermore they also account for the transmission factors derived from the wall loss rates that have been determined for $H_2SO_4$ and so far separately for $HO_2$, $CH_3O_2$, $C_2H_5O_2$, and $C_3H_7O_2$ in the laboratory [17,21,22]. Since only two measurements with $N_2$ and $O_2$ buffer, respectively, are carried out, only two quantities are obtained. Hence Eq. (3) has to be reduced to two unknowns. This can be achieved by introducing a "reference" peroxy radical, i.e. by assuming that all $R_iO_2$ behave like this radical with regard to chemical conversion in the respective buffer gas. At least in the clean and free troposphere $CH_3O_2$ is the most abundant $RO_2$ and has been selected as reference radical. From Eq. (3) the following expressions for [$\Sigma RO_2$] and [$HO_2$] are derived

$$[\Sigma RO_2] = \frac{[H_2SO_4]_{N_2-buffer} - [H_2SO_4]_{O_2-buffer}}{\alpha_{CH_3O_2}(\mathrm{CE}_{N_2-buffer} - \mathrm{CE}_{O_2-buffer})} = \frac{\Delta[H_2SO_4]}{\alpha_{CH_3O_2}(\mathrm{CE}_{N_2-buffer} - \mathrm{CE}_{O_2-buffer})} \quad (4)$$

$$[HO_2] = \frac{[H_2SO_4]_{N_2-buffer} - \Delta[H_2SO_4]^* \dfrac{\mathrm{CE}_{N_2-buffer}}{\mathrm{CE}_{N_2-buffer} - \mathrm{CE}_{O_2-buffer}}}{\alpha_{HO_2}} \quad (5)$$

This estimate gives an upper limit for [$HO_2$] and a lower limit for [$\Sigma RO_2$]. This will be discussed in more detail below. Typical values of CE are around 90% for the $O_2$ buffer and between 25% and 30% for the $N_2$ buffer.

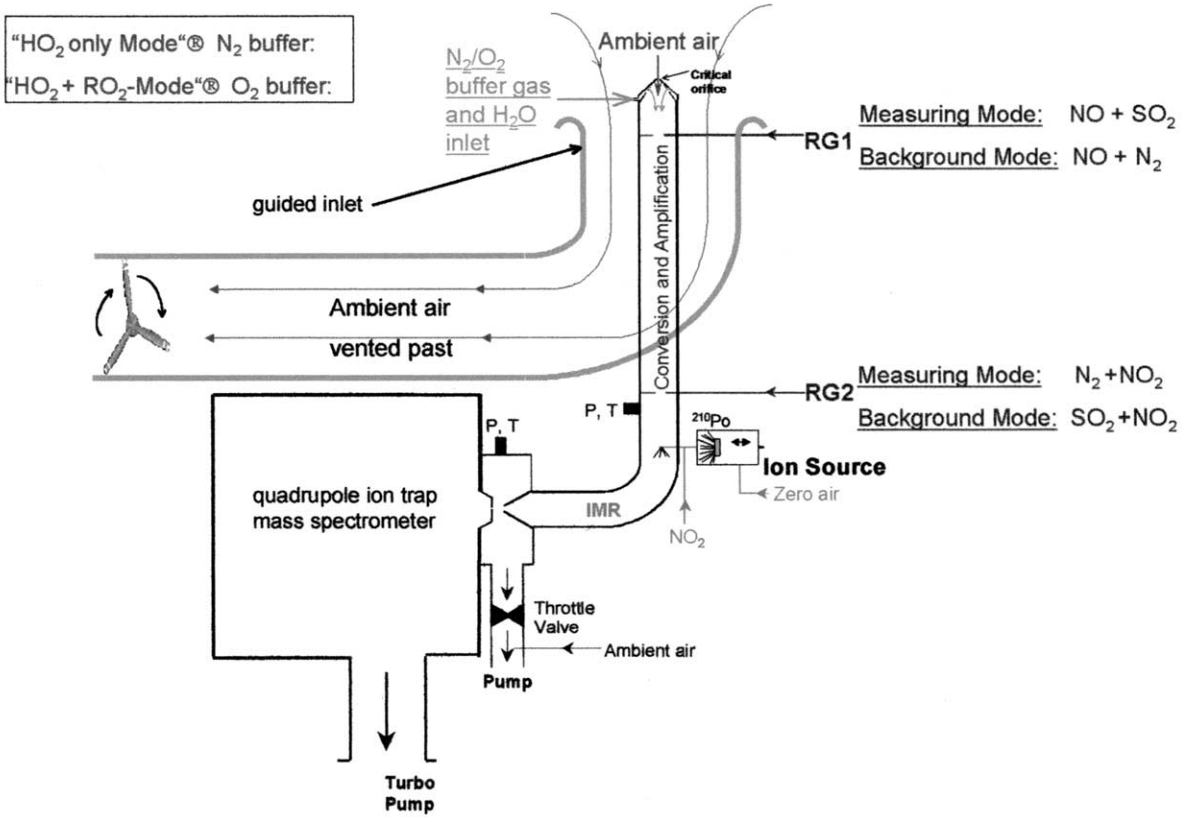


Fig. 2. The experimental setup of ROxMAS that has been used for the recent field measurements. RG1, RG2: reagent gas inlet ports, p: pressure sensor, T: temperature sensor, IMR: ion molecule reaction section. For further details see text.

The detection of $H_2SO_4$ by CIMS [21–31] employs the gas-phase ion molecule reaction of $H_2SO_4$ with gaseous $NO_3^-(HNO_3)_n$ ions

$$NO_3^-(HNO_3)_n + H_2SO_4 \rightarrow HSO_4^-(HNO_3)_n + HNO_3 \quad (6)$$

which was originally proposed by [25], and subsequently investigated in the laboratory [26,27]. The concentration of $H_2SO_4$ is obtained from the observed abundance ratio R of the product ions $HSO_4^-(HNO_3)_n$ and the reactant ions $NO_3^-(HNO_3)_n$, using the reaction kinetics of Eq. (6) [17,25,28,29].

### 2.2. Instrumental

The experimental setup of ROxMAS is shown in Fig. 2. The main components of ROxMAS are a stainless-steel FR tube (4 cm inner diameter ID, thermostated at ~18°C) with a buffer- and sample-gas inlet at the beginning of the tube and reagent-gas inlets further downstream, an ion source, and a quadrupole ion-trap mass spectrometer. The impact of wall losses of the highly reactive peroxy radicals before entering the detection region is minimized by embedding the ROxMAS flow reactor (FR) in a guided inlet system, through which ambient air is pulled with a velocity of about 10 m/s past the FR through a blower. Due to the pressure gradient between the FR (in the FR a pressure of 280–300 mbar is maintained) and the atmosphere, a small portion of ambient air (flow rate 1.3 l/min at standard temperature and pressure = 1.3 slm) is drawn into the FR through a critical orifice (radius 0.19 mm). Right after the critical orifice the atmospheric air is diluted in

either $N_2$ or $O_2$, which is added through a conical multihole inlet port.

Downstream (6 cm) NO (0.056 slm, 400 ppm in $N_2$) and $SO_2$ (0.5–1 slm, 4000 ppm or 2000 ppm in $N_2$, respectively) are co-added through reagent-gas inlet port 1 (RG1). RG1 consists of two stainless-steel injector needles (0.1 cm ID, 0.25 cm OD) protruding to the center of the tube with the openings pointing vertical to the flow direction. The turbulence caused by the injection of the buffer and reagent gases leads to a fast mixing.

From RG1 downstream within the conversion and amplification section, the ratio of buffer and reagent gases to sample gas is ~9. Including the pressure reduction the sampled air is diluted by a factor of about 21–27. The degree of dilution further reduces the impact of possible interference processes on the chemical conversion and amplification mechanism such as the reaction of $HO_x$ with ambient $NO_2$ as already mentioned above.

A flow of $N_2$, equal to the flow of $SO_2$, is added 60 cm downstream of RG1 through RG2, which is identical with RG1. This is necessary for background measurements performed periodically to capture $H_2SO_4$ or $HSO_4^-$ signals originating from sources other than ambient peroxy radicals [17,18,21]. The background is determined by switching (controlled by a dual-valve arrangement) $SO_2$ from RG1 to RG2 and substituting $SO_2$ at RG1 with the $N_2$ from RG2, while NO is still added through RG1 to convert atmospheric peroxy radicals to HONO (Fig.1). This procedure maintains the same flow conditions at RG1 and RG2 for both measurement modes, eliminates pressure pulses, and keeps the conditions in the IMR section unchanged.

To check for possible interference from peroxy radicals resulting from thermal decomposition of PAN or $HNO_4$, whose concentrations may reach relatively high values in particular in the colder regions of the middle and upper troposphere [32,33], $SO_2$ can be also switched to an auxiliary reagent-gas inlet port (ARG) (not shown in Fig.1) about 16 cm downstream of RG1 while still adding NO through RG1. Between RG1 and the ARG atmospheric peroxy radicals are converted to HONO as described above, yet downstream of ARG again $SO_2$ and NO are present, hence any peroxy radicals produced in the flow reactor downstream will therefore be measured as background signal. During the measuring campaign on MTC (see below), however, no significant signals, which might result from the decomposition of PAN or $HNO_4$, could be observed.

$H_2O$ ($\sim 5 \times 10^{16}$ $cm^{-3}$) is added along with the buffer gas in order to efficiently convert $SO_3$ to $H_2SO_4$ [17–21]. Apart from this, the added water makes the system less susceptible to atmospheric changes [21], thus enabling a stable operation. To ensure that the chain reaction has terminated as the air reaches RG2, $NO_2$ is added through RG2 (0.23 slm 2500 ppm in $N_2$).

At a distance of 11.5 cm downstream of RG2, $NO_3^-(HNO_3)_n$ ions are injected into the flow tube. The ionization is spatially separated from the main gas flow by a capillary tube, which is flushed by the source gas composed of 2.2 slm synthetic air (purity 5.0) and 0.1 slm pure $NO_2$. The $NO_3^-(HNO_3)_n$ reactant ions in the source gas are produced either by $\alpha$ bombardment from a $^{210}Po$ (65 MBq, 5.4 MeV) source, or by a high-frequency glow-discharge capillary-tube ion source commonly used by our group [15–21,30,31]. Reaction of $H_2SO_4$ with $NO_3^-(HNO_3)_n$ ions takes place between the ion-source gas inlet and the second critical orifice (radius: 1.18 mm, distance: 46 cm), through which the ions enter the second pumping stage where a pressure of around 50–80 mbar is maintained by a mechanical pump and a throttle valve. After 2.5 cm, the ions enter the high-vacuum recipient of the quadrupole ion-trap mass spectrometer [21,34] through a 0.15 mm diameter inlet orifice, where they are mass-selected and detected.

To achieve a high time resolution and not to lose too much information with respect to the buffer mode, which is off, while the other mode is on, the buffer gases have to alternate rapidly (within the lifetime of atmospheric peroxy radicals, on the order of 1 min). Dead space in the gas lines is minimized using direct connections and low-dead-space pneumatic valves. Fast switching between the two buffer gases or to the background mode is realized by computer control

(Labview). In this way a duty cycle of about 120 s is realized, 50 s for the $HO_2$-only mode, 10 s which are required for the transition from $N_2$ to $O_2$ buffer (and vice versa) and stabilization of the system, 50 s $HO_2 + RO_2$ mode, and 10 s again for stabilization. The background mode is run after every 30th cycle.

### *2.3. Calibration and diagnostics*

Calibration and diagnostic measurements aimed at characterizing the flow-reactor system and the mass-spectrometer system as completely as possible, i.e. determining a calibration factor consisting of several independent factors, among these the most important are the transmissions of different sections of the FR [19,21,22].

The principle of our calibration source is based on the photolysis of $H_2O$ at 184.9 nm in purified zero air producing 50% OH and 50% $HO_2$. For producing 100% $HO_2$ sufficient amounts of CO are added to the gas flow to convert all OH radicals to $HO_2$. Furthermore, there is the possibility to produce $RO_2$ along with $HO_2$ by replacing CO with a suitable hydrocarbon (RH) like e.g. $CH_4$ to produce $CH_3O_2$. Previously we determined the $HO_x$ concentrations produced by the radical source by measuring the $O_3$ production from the photolysis of $O_2$ at the same wavelength, i.e. the lamp fluence is calibrated by ozone actinometry. [19,21,35]. The determination of the $HO_x$ concentration by $O_3$ actinomtery, however, implies some disadvantages, such as the determination of an effective absorption cross section for the $O_2$ photolysis for the specific measuring conditions [36,37] or the necessity of relatively high lamp intensities which has the effect that the calibration source can be only operated with trace quantities of water vapor ($\leq$1000 ppmv).

Recently we improved and modified the system in such a way that it can be operated at water vapor contents between 500 ppmv and atmospheric ground-level values. This has been achieved by measuring the lamp flux with a calibrated UV photodiode instead of $O_3$ actinometry. This setup will be discussed in a forthcoming paper. The new calibration unit allowed us to check the influence of higher relative humidities (typical atmospheric values) on the response of the ROxMAS system. This test was important because with respect to another amplifier technique, PERCA box (NO/CO chemical amplifier), Mihele and Hastie [38] reported that the chain length of the PERCA mechanism decreases with increasing water vapor content in the reactor. Varying the humidity in the calibration source between 0.9% and ambient water vapor levels has not shown any significant effect of humidity on the calibration factor and thus on the response of the ROxMAS system [21].

Apart from these studies further diagnostic measurements, such as calibration of the instrument for different ambient conditions, determination of wall losses and conversion efficiencies separately for $HO_2$, $CH_3O_2$, $C_2H_5O_2$, and $C_3H_7O_2$, were carried out and will also be described in the forthcoming paper.

## 3. Results and discussion

Within the framework of the project MINATROC (Mineral dust And Tropospheric Chemistry), long-term ground-based measurements were carried out at the WMO station on the summit of Monte Cimone (MTC) (44° 11′ N - 10° 42′ E, 2165 m asl), Italy, between June and July 2000.

The diurnal profiles of the measured volume mixing ratios of $HO_2$ (●), $\Sigma RO_2 + HO_2$ (▼) and the derived volume mixing ratio of $\Sigma RO_2$ (□) obtained on 22nd June 2000 are shown in Fig. 3 (upper panel). This day was a cloud-free summer day with relative humidities below 65%, a noon-time temperature of 18°C, and south-westerly winds with velocities of about 6 m/s. The symbols represent 30-min averages and the lines 1-min time-resolved data. From instrumental uncertainties only, the $2\sigma$ precision is estimated to be 7% and the accuracy 30%, mainly due to uncertainties resulting from the calibration. For the conditions on 22nd June we determined empirically by means of calibration measurements a CE of 88% in $O_2$ buffer and a CE of 28% in $N_2$ buffer for the "reference" peroxy radical $CH_3O_2$. These CE values correspond pretty well with the theoretical values derived from Eq. (2) for the operational conditions.

The measured distinct diurnal cycle of peroxy

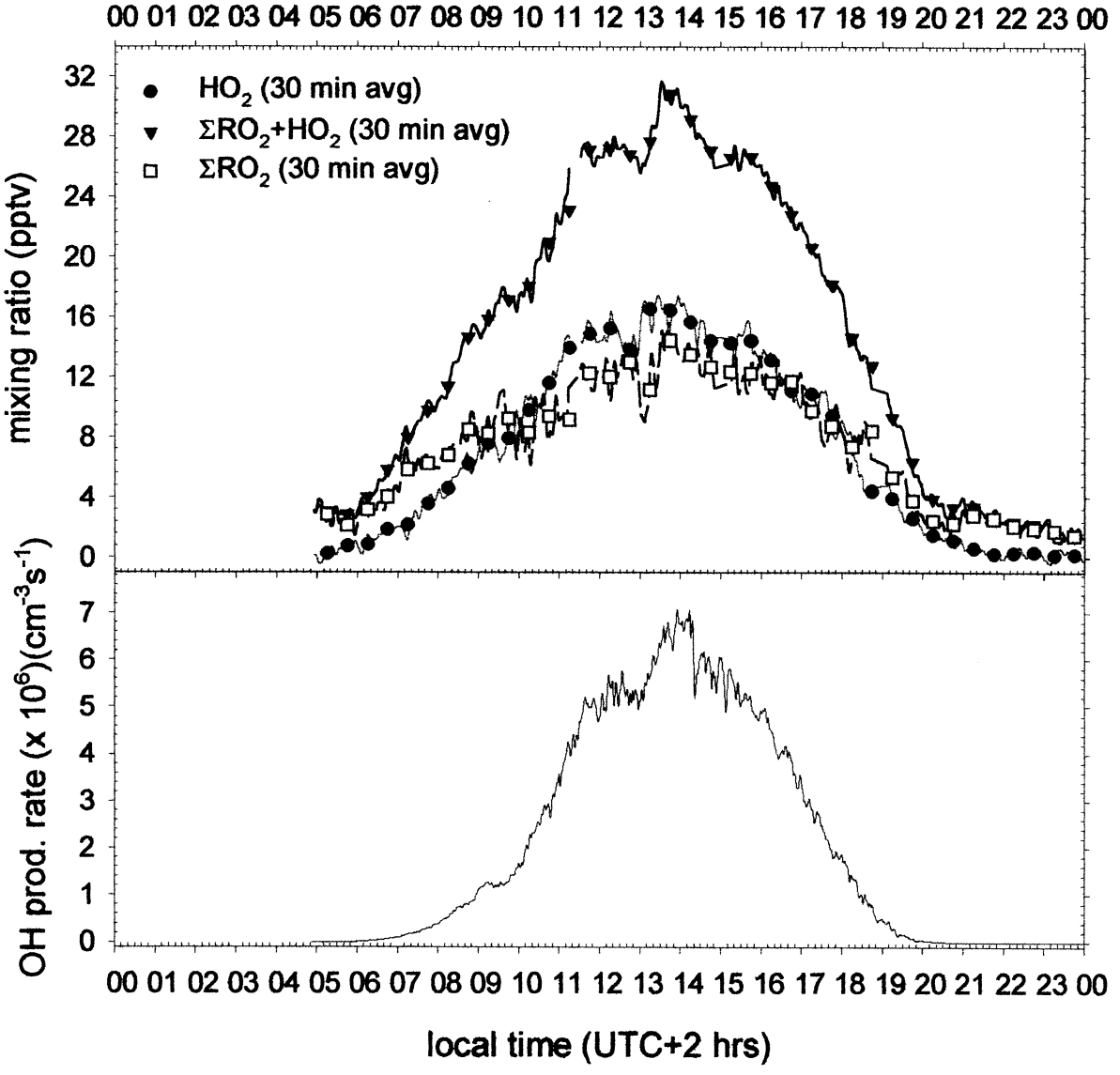


Fig. 3. Upper panel: Diurnal profiles of the measured volume mixing ratios of $HO_2$ (●), $\Sigma RO_2 + HO_2$(▼) and the derived volume mixing ratio of $\Sigma RO_2$ (□) obtained on 22nd June 2000 on Monte Cimone, Italy. Lower panel: Production rate of OH. For further details see text.

radicals with a midday maximum clearly indicates their photochemical origin. Since the atmospheric radical cycling reactions establish a fast photochemical steady state between OH, $HO_2$, and $RO_2$, a good correlation might be expected between $[HO_2 + \Sigma RO_2]$ and the production rate of OH (lower panel of Fig.3, determined from $J(O(^1D))$ (measured by MPI-C, Mainz), $[O_3]$ and $[H_2O]$). This is confirmed by the observed data. Even highly time-resolved distinct features of the production rate can be seen in the highly time-resolved profile of $[HO_2 + \Sigma RO_2]$. The midday maxima are $[HO_2 + \Sigma RO_2] = 32$ pptv, $[HO_2] = 17$ pptv, and $[\Sigma RO_2] = 15$ pptv. The noontime ratio $[\Sigma RO_2]/[HO_2] \approx 1$ would be consistent to a first approximation with photostationary-state calculations for relatively "chemically clean" air conditions

and $CH_3O_2$ being the predominant $RO_2$ [cf. 39–41]. These conditions are in agreement with the supplementary measurements carried out by our MINATROC partner MPI-C, Mainz, on MTC [NO] <70 pptv (between 10 a.m. and 7 p.m. mean value 47 pptv with a variability of 12 pptv), [CO] ≈ 100 ppbv). Before sunrise and after sunset the $[HO_2]$ level is at or below detection limit (0.5 pptv), whereas $[\Sigma RO_2]$ is clearly above. For these particular $NO_x$-poor conditions, the rapid loss of $[HO_2]$ after sunset and the tail effect of $RO_2$ due to the longer lifetime of $CH_3O_2$ can be reproduced considering the loss of peroxy radicals only by self- and cross-reactions [cf. 42]. The $[\Sigma RO_2]$ of almost 4 pptv just before sunrise demonstrates that there was night-time oxidation chemistry taking place [42,43].

On 22nd June low $NO_x$ values, the approximate $[\Sigma RO_2]/[HO_2]$ ratio of 1:1 and the relatively fast tailing of $[\Sigma RO_2]$ after sunset are rather an indication for simple radical chemistry with $CH_3O_2$ being the predominant organic radical for this specific day. Therefore, under these chemically "clean", i.e. relatively unpolluted, atmospheric conditions, the uncertainty associated with the approach of using $CH_3O_2$ as a "reference" peroxy radical is expected to be relatively low. This also holds for any $RO_2$ radical which is converted to $HO_2$ via $CH_3O_2$ and thus shows a similar discrimination as $CH_3O_2$ [21]. For example such an $RO_2$ radical would be the acetyl peroxy radical $CH_3C(O)O_2$ resulting from either photodissociation of acetone, which can be a significant $RO_x$ source in the upper troposphere [44–46], or thermal decomposition of peroxyacetyl nitrate (PAN), an important $NO_x$ and $RO_2$ reservoir, which is formed in either polluted environments or in locations with low temperatures and can be transported to less polluted areas and/or warmer locations where it thermally decomposes [32]. Under other conditions, e.g. "not so clean" boundary-layer conditions, where other $RO_2$ radicals might be important, our methodology may underestimate $[RO_2]$ and overestimate $[HO_2]$, because the degree of discrimination for many $RO_2$ species is likely to be lower than for $CH_3O_2$ [personal communication with Jenkin, 21]. With respect to later atmospheric conditions, presently uncertainty studies are carried out both in the laboratory and theoretically. So far first estimates show a maximum uncertainty of 20% for both $[HO_2]$ and $[\Sigma RO_2]$. For this estimate theoretical $RO_2$ radical distributions reported by Madronich and Calvert [47] for a clean marine boundary-layer case and a continental Amazon boundary-layer case, and a radical distribution measured by Mihelcic et al. [48], on the Schauinsland in the Black Forest were compared to the case 100% $CH_3O2$ of which the CE has been used to derive $[HO_2]$ and $[\Sigma RO_2]$ [21].

The example presented demonstrates that ROx-MAS with its high time resolution and its capability of speciated measurements is, at least under "clean" chemical atmospheric conditions, a powerful tool to investigate the fast atmospheric radical chemistry and to give an insight into the interconversion reactions. So far this unique measurement capability of ROx-MAS, though with a lower time resolution, has been offered only by the MIESR (matrix isolation spin resonance) technique that is not an on-line method.

## Acknowledgements

The authors would like to thank the MINATROC community and the technical staff of MPI-K. Also special thanks to G. Hönes. Parts of this work were funded by EU (EVK2-CT-1999-00003).

## References

[1] J.A. Logan, M.J. Prather, S.C. Wofsy, M.B. McElroy, J. Geophys. Res. 86 (1981) 7210.
[2] J.H. Seinfeld, S.N. Pandis, Atmospheric Chemistry and Physics, John Wiley and Sons, New York, 1997.
[3] I. Bey, B. Aumont, G. Taumont, J. Geophys. Res. 106 (2001) 9991.
[4] T.M. Hard, C.Y. Chan, A.A. Mehrabzadeh, R.J. O'Brien, J. Geophys. Res. 97 (1992) 9785.
[5] M.R. Heal, D.E. Heard, M.J. Pilling, B.J. Whitaker, J. Atmos. Sci. 52 (1995) 3428.
[6] D.J. Creasey, D.E. Heard, P.A. Halford-Maw, M.J. Pilling, B.J. Whitaker, J. Chem. Soc., Faraday Trans. 29 (1997) 93.
[7] W.H. Brune, P.S. Stevens, J.H. Mather, J. Atmos. Sci. 52 (1995) 3328.
[8] P.S. Stevens, J.H. Mather, W.H. Brune, J. Geophys. Res. 99 (1994) 3543.
[9] P.O. Wennberg, R.C. Cohen, N.L. Hazen, L.B. Lapson, N.T.

Allen, T.F. Hanisco, J.F. Oliver, N.W. Lanham, J.N. Denusz, J.G. Anderson, Rev. Sci. Instrum. 65 (1994) 1858.
[10] P.O. Wennberg, T.F. Hanisco, R.C. Cohen, R.M. Stimpfle, L.B. Lapson, J.G. Anderson, J. Atmos. Sci. 52 (1995) 3413.
[11] C.A. Cantrell, D.H. Stedman, Geophys. Res. Lett. 9 (1982) 846.
[12] C.A. Cantrell, D.H. Stedman, G.J. Wendel, Anal. Chem. 56 (1984) 1496.
[13] K.C. Clemitshaw, L.J. Carpenter, S.A. Penkett, M.E. Jenkin, J. Geophys. Res. 102 (1997) 25405.
[14] D. Mihelcic, D. Klemp, P. Müsgen, H.W. Pätz, A. Volz-Thomas, J. Atmos. Chem. 16 (1993) 313.
[15] T. Reiner, M. Hanke, F. Arnold, Proceedings of EUROTRAC Symposium 1996, Garmisch-Partenkirchen, Computational Mechanics Publications, 1996, p. 633.
[16] T. Reiner, Dissertation, University of Heidelberg (1994).
[17] T. Reiner, M. Hanke, F. Arnold, J. Geophys. Res. 102 (1997) 1311.
[18] T. Reiner, M. Hanke, F. Arnold, Geophys. Res. Lett. 25 (1998) 47.
[19] T. Reiner, M. Hanke, F. Arnold, H. Ziereis, H. Schlager, W. Junkermann, J. Geophys. Res. 104 (1999) 18647.
[20] T. Reiner, M. Hanke, F. Arnold, H. Ziereis, H. Schlager, W. Junkermann, Proceedings of EUROTRAC Symposium 1998, Garmisch-Partenkirchen, Computational Mechanics Publications, 1999, p. 392.
[21] M. Hanke, Dissertation, University of Heidelberg (1999).
[22] M. Hanke, J. Uecker, J. Reimann, T. Reiner, F. Arnold, Proceedings of EUROTRAC Symposium ’2000, Garmisch-Partenkirchen, Computational Mechanics Publications, (2000) 1376.
[23] P.D. Lightfoot, R.A. Cox, J.N. Crowley, M. Destriau, G.D. Hayman, M.E. Jenkin, G.K. Moortgat, F. Zabel, Atmos. Environ., 26A-10 (1992) 1805.
[24] R. Atkinson, D.L. Baulch, R.A. Cox, J.R.F. Hampson, J.A. Kerr, M.J. Rossi, J. Troe, J. Phys. Chem. Ref. Data 26 (1997).
[25] F. Arnold, R. Fabian, Nature 283 (1980) 55.
[26] A.A. Viggiano, R.A. Perry, D.L. Albritton, E.E. Ferguson, F.C. Fehsenfeld, J. Geophys. Res. 87 (1982) 7340.
[27] A.A. Viggiano, J.V. Seeley, P.L. Mundis, J.S. Williamson, R.A. Morris, J. Phys. Chem. A 101 (1997) 8275.
[28] O. Möhler, Th. Reiner, F. Arnold, Rev. Sci. Instrum. 64 (1993) 1199.
[29] D.J. Tanner, F.L. Eisele, J. Geophys. Res. 100 (1995) 2883.
[30] O. Möhler, F. Arnold, J. Atmos. Chem. 16 (1991) 33.
[31] T. Reiner, F. Arnold, J. Chem. Phys. 101 (1994) 7399.
[32] H.B. Singh, D. Herlth, D. O’Hara, K. Zahnle, J.D. Bradshaw, S.T. Sandholm, R. Talbot, J. Crutzen, M. Kanakidou, J. Geophys. Res. 97 (1992) 16523.
[33] M. Kanakidou, H.B. Singh, K.M. Valentin, P.J. Crutzen, J. Geophys. Res. 96 (1991) 15395.
[34] A. Kiendler, S. Aberle, F. Arnold, Atmos. Environ. 34 (2000) 2623.
[35] M. Schultz, M. Heitlinger, D. Mihelcic, A. Volz-Thomas, J. Geophys. Res. 100 D9 (1995) 18811.
[36] E.J. Lanzendorf, T.F. Hanisco, N.M. Donahue, P.O. Wennberg, Geophys. Res. Lett. 24 (1997) 3037.
[37] A. Hofzumahaus, T. Brauers, U. Aschmutat, U. Brandenbruger, H.-P. Dorn, M. Hausmann, M. Heßling, P. Holland, C. Plass-Dülmer, M. Sedpacek, M. Weber, D. H. Ehhalt, Geophys. Res. Lett. 24 (1997) 3039.
[38] C.M. Mihele, D.R. Hastie, Geophys. Res. Lett. 25,11 (1998) 1911.
[39] C.A. Cantrell, J.A. Lind, R.E. Shetter, J.G. Calvert, P.D. Goldan, W. Kuster, F.C. Fehsenfeld, S.A. Montzka, D.D. Parrish, E.J. Williams, M.P. Buhr, H.H. Westberg, G. Allwine, R. Martin, J. Geophys. Res., 97 (1992) 20671.
[40] B.A. Ridley, S. Madronich, R.B. Chatfield, J.G. Walega, R.E. Shetter, M.A. Carroll, D.D. Montzka, J. Geophys. Res. 97 (1992) 10375.
[41] P.S. Stevens, J.H. Mather, W.H. Brune, F. Eisepe, D. Tanner, A. Jefferson, C. Cantrell, R. Shetter, S. Sewall, A. Fried, B. Henry, E. Williams, K. Baumann, P. Goldan, W. Kuster, J. Geophys. Res. 102 (1997) 6379.
[42] P.S. Monks, L. Carpenter, S.A. Penkett, Geophys. Res. Lett. 23 (1996) 535.
[43] U. Platt, G. LeBras, G. Poulet, J.H. Burrows, G. Moortgat, Nature 348 (1990) 147.
[44] F. Arnold, V. Bürger, B. Droste-Franke, F. Grimm, A. Krieger, J. Schneider, T. Stilp, Geophys. Res. Lett. 24 (1997) 3017.
[45] T. Reiner, O. Möhler, F. Arnold, J. Geophys. Res. 104 (1999) 13943.
[46] K.-H. Wohlfrom, T. Hauler, F. Arnold, H. Singh, Geophys. Res. Lett. 26 (1999) 2849.
[47] S. Madronich, J.G. Calvert, J. Geophys. Res. 95 (1990) 5697.
[48] D. Mihelcic, A. Volz-Thomas, H.W. Pätz, D. Kley, M. Mihelcic, J. Atmos. Chem. 11 (1990) 271.